



Australian Journal of Earth Sciences

An International Geoscience Journal of the Geological Society of Australia

ISSN: (Print) (Online) Journal homepage: www.tandfonline.com/journals/taje20

P–*T* conditions of metamorphic and hydrothermal events at Tick Hill Gold Deposit, Mount Isa, Queensland, Australia

T. X. Le, P. H. G. M. Dirks, I. V. Sanislav, J. M. Huizenga, H. A. Cocker & G. T. T. Nguyen

To cite this article: T. X. Le, P. H. G. M. Dirks, I. V. Sanislav, J. M. Huizenga, H. A. Cocker & G. T. T. Nguyen (17 Mar 2024): *P*–*T* conditions of metamorphic and hydrothermal events at Tick Hill Gold Deposit, Mount Isa, Queensland, Australia, Australian Journal of Earth Sciences, DOI: [10.1080/08120099.2024.2320195](https://doi.org/10.1080/08120099.2024.2320195)

To link to this article: <https://doi.org/10.1080/08120099.2024.2320195>



© 2024 The Author(s). Published by Informa UK Limited, trading as Taylor & Francis Group.



[View supplementary material](#)



Published online: 17 Mar 2024.



[Submit your article to this journal](#)




[View related articles](#)



[View Crossmark data](#)

P–*T* conditions of metamorphic and hydrothermal events at Tick Hill Gold Deposit, Mount Isa, Queensland, Australia

T. X. Le^{a,b} , P. H. G. M. Dirks^b , I. V. Sanislav^b , J. M. Huizenga^{b,c,d} , H. A. Cocker^b  and G. T. T. Nguyen^e

^aFaculty of Geosciences and Geology Engineering/CEAE (Center for Excellence in Analysis and Experiment), Hanoi University of Mining and Geology, Bac Tu Liem, Hanoi, Vietnam; ^bEGRU (Economic Geology Research Centre), College of Science and Engineering, James Cook University, Townsville, QLD, Australia; ^cFaculty of Environmental Sciences and Natural Resource Management, Norwegian University of Life Sciences, Ås, Norway; ^dDepartment of Geology, University of Johannesburg, Johannesburg, South Africa; ^eFaculty of Geology, VNU-HCM University of Science, Ho Chi Minh, Vietnam

ABSTRACT

Tick Hill Gold Deposit is a unique gold mineralisation style in the Mary Kathleen Fold Belt in the Mount Isa Inlier. The gold at Tick Hill is generally pure without silver and was formed during two discrete metamorphic–deformation events (*D*₁ and *D*₃). Early gold was observed as inclusions or coarse grains hosted within *D*₁ peak-metamorphic diopside, scapolite and hornblende from the garnet–biotite–hornblende (tschermakite)–plagioclase (andesine)–quartz assemblage. Late gold is closely associated with bismuth selenide, chlorite, albite, sericite and K-feldspar, and formed during *D*₃. The syn-*D*₁ garnet–plagioclase–hornblende–quartz–biotite assemblage was used to constrain the pressure and temperature (*P*–*T*) conditions of metamorphism and mineralisation using the garnet–plagioclase–hornblende–quartz barometer and the hornblende–plagioclase, garnet–biotite and garnet–hornblende thermometers. The results show that peak metamorphism at Tick Hill reached *P*–*T* conditions of 6.0–7.6 kbar and 720–760 °C. These *P*–*T* conditions together with gneissic and migmatite textures recorded in different rock types at the Tick Hill area indicate that the peak metamorphism preserved in the area occurred at the amphibolite–granulite facies, compared with the amphibolite facies at the southern Mary Kathleen and Eastern Fold Belt. The *D*₃ chlorite, which formed during stage 2 to stage 4 mineralisation events, displays a wide range of compositions reflecting a gradual retrograde temperature change from ~380 °C to ~130 °C. The pressures during *D*₃ could not be reliably determined, but the presence of various Bi-selenides suggests that towards the waning stages of *D*₃, the rocks may have been exhumed to a pressure less than 1 kbar.

KEY POINTS

1. The 1790–1770 Ma *D*₁ peak metamorphism at Tick Hill reached 6–7.6 kbar and 720–760 °C.
2. The 1525–1520 Ma *D*₃ hydrothermal mineralisation at Tick Hill Deposit occurred at temperatures between ~380 °C and ~130 °C.
3. The main *D*₃ gold accumulation episodes at Tick Hill occurred at temperatures ranging from ~380 to 160 °C.

ARTICLE HISTORY

Received 19 June 2023
Accepted 6 February 2024

KEYWORDS



Tick Hill; gold deposit; Mary Kathleen; Mount Isa; geobarometry; geothermometry


Introduction

The Tick Hill deposit is situated in the southern Mary Kathleen Domain in the Mount Isa Inlier (northeast Queensland, Australia; Figure 1). The high grade of the single-orebody deposit, the lack of sulfides and the presence of almost exclusively free gold within upper-amphibolite facies, quartz–feldspar mylonite units, make Tick Hill a unique gold deposit in the Mount Isa Inlier. Gold mineralisation is hosted in a sequence, from proximal outward, consisting of quartz–feldspar mylonite, biotite schist (±calc-silicate gneiss), quartzite, calc-silicate and amphibolite (Le *et al.*, 2021a). These rocks were affected by

1790–1770 Ma *D*_{1–2} shearing and folding at amphibolite–granulite metamorphic facies, followed by 1525–1520 Ma *D*₃ metamorphism and hydrothermal events with widespread quartz–feldspar alteration and the latest *D*₄ strike-slip faulting (Le *et al.*, 2021a, 2021b). The metamorphic sediments in the Tick Hill area were intruded by *D*_{1–2} granite and leucogranite and *D*₃ pegmatite (Figure 2; Le *et al.*, 2021a, 2021b).

Gold mineralisation at Tick Hill formed during two discrete events, syn-*D*₁ and syn-*D*₃. Early gold occurs as inclusions intergrown with syn-*D*₁ peak-metamorphic minerals (*i.e.* diopside, scapolite and hornblende), whereas late gold is hosted within quartz–feldspar mylonite and intensely silicified units, which were

CONTACT T. X. Le  lexuantruong@humg.edu.vn  Faculty of Geosciences and Geology Engineering/CEAE (Center for Excellence in Analysis and Experiment), Hanoi University of Mining and Geology, 18 Pho Vien, Bac Tu Liem, Hanoi, Vietnam

 Supplemental data for this article can be accessed online at <https://doi.org/10.1080/08120099.2024.2320195>.

Editorial handling: Anita Andrew

© 2024 The Author(s). Published by Informa UK Limited, trading as Taylor & Francis Group.

This is an Open Access article distributed under the terms of the Creative Commons Attribution-NonCommercial-NoDerivatives License (<http://creativecommons.org/licenses/by-nc-nd/4.0/>), which permits non-commercial re-use, distribution, and reproduction in any medium, provided the original work is properly cited, and is not altered, transformed, or built upon in any way. The terms on which this article has been published allow the posting of the Accepted Manuscript in a repository by the author(s) or with their consent.

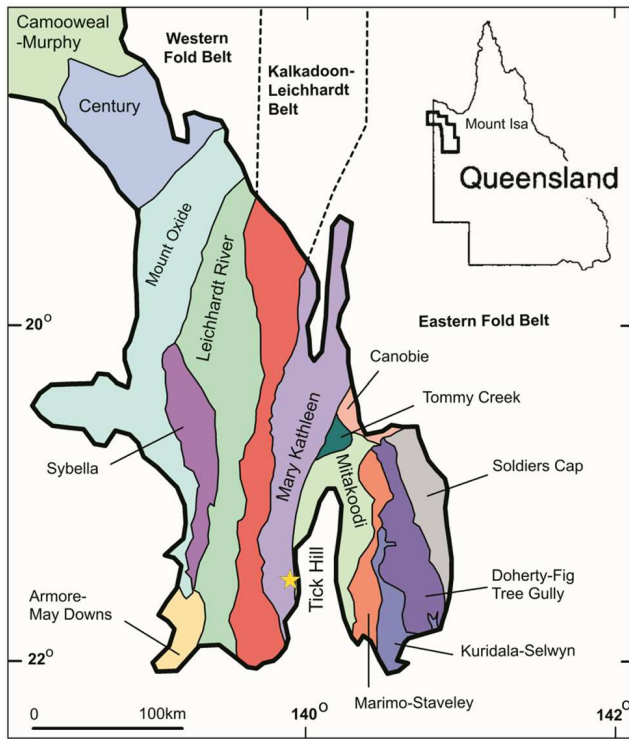


Figure 1. Tectonic subdivisions of the Mount Isa Inlier, as defined by Withnall and Hutton (2013), showing the location of Tick Hill Deposit. The insert map shows the location of the Mount Isa Inlier in relation to Queensland.

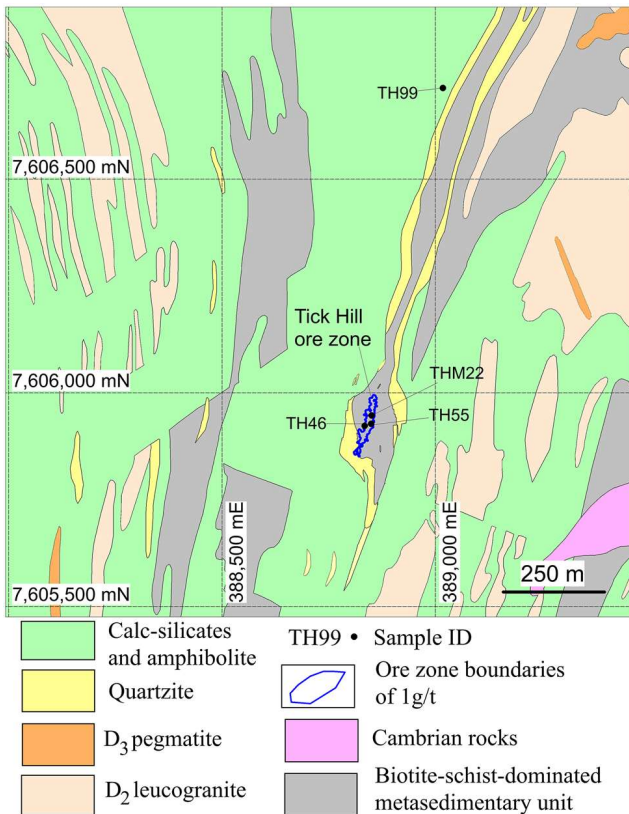


Figure 2. Geology map of local study area showing locations of mineral geochemistry samples at the Tick Hill area (adapted from Le *et al.*, 2021a; Rutherford, 2000; Wyborn, 1997). The datum is Zone 54-GDA94. Samples TH46 and TH99 were collected from drill cores, whereas samples TH55 and THM22 were collected from the mining pit at different levels.

affected by D_3 fracturing and associated alteration (Le *et al.*, 2021a). Minerals aligned in the early D_1 fabric define the peak-metamorphic assemblage (e.g. garnet–amphibole–biotite–plagioclase in meta-amphibolite; diopside–scapolite–amphibole–plagioclase in calc-silicate; sillimanite–biotite–K-feldspar–plagioclase–quartz in metapelite; Le *et al.*, 2021a) in which gold was locally hosted in S_1 -aligned diopside, hornblende and scapolite (Le *et al.*, 2021a). During D_3 , the peak assemblages were overprinted by retrograde mineral assemblages that typically include albite–hornblende/actinolite–epidote–chlorite–hematite–quartz and later sericite–K-feldspar–calcite–clay minerals. Both mineral assemblages were associated with the redistribution of earlier gold and the possible introduction of a new phase of gold (Le *et al.*, 2021a). D_3 alteration involved the local destruction of magnetite, the emplacement of abundant laminar quartz veins and the deposition of multi-stage alteration assemblages (Le *et al.*, 2021a), including:

- Stage 1: quartz–oligoclase–albite–hornblende–hematite (\pm leucoxene, chalcopyrite);
- Stage 2: albite–actinolite–chlorite₁–hematite (\pm leucoxene)–pyrrhotite–pyrite₁–chalcopyrite–gold–bismuth selenide;
- Stage 3: quartz–K-feldspar–chlorite₂–epidote–sericite–hematite (\pm leucoxene)–gold–bismuth selenide–pyrite₂–chalcopyrite;
- Stage 4: quartz–calcite–chlorite₃–clay minerals–hematite (\pm leucoxene)–gold–pyrite–chalcopyrite–Bi, Pb, Cu selenides including juninite ($Pb_3Cu_2Bi_8(S,Se)_{16}$), cerrromonjonite ($CuPbBiSe_3$) and molybdomenite ($PbSeO_3$); and
- Stage 5: quartz–albite–oligoclase–magnetite.

Apart from the recent investigations conducted by Le *et al.* (2021a, 2021b, 2022) on the effects and timing of deformation (referred to as D_{1-3}) and mineralisation events in the Tick Hill area, there is a scarcity of studies on the geological history, metamorphic–tectonic processes and mineralisation in the southern Mary Kathleen region. Interpretations of the metamorphic and hydrothermal conditions for the region are mainly based on the studies of (1) the occurrence of metamorphic and hydrothermal alteration mineral assemblages and petrographic textures (Le *et al.*, 2021a) and (2) implications of quartz oxygen isotopic values (Le *et al.*, 2022). The pressure–temperature (P – T) conditions for these events have not been quantified. In this study, we evaluate the P – T conditions of the D_{1-2} peak metamorphism, mineralisation and D_3 deformation events at Tick Hill gold deposit using (1) garnet–plagioclase–hornblende–quartz barometry, (2) hornblende–plagioclase thermometry, (3) garnet–biotite thermometry, (4) garnet–hornblende thermometry and (5) chlorite thermometry, based on major-element mineral geochemistry obtained from an electron probe micro-analysis (EPMA).

Sample descriptions

This study focuses on three rock types containing mineral assemblages that are appropriate for geothermobarometry and occur in direct association with gold. These include amphibole

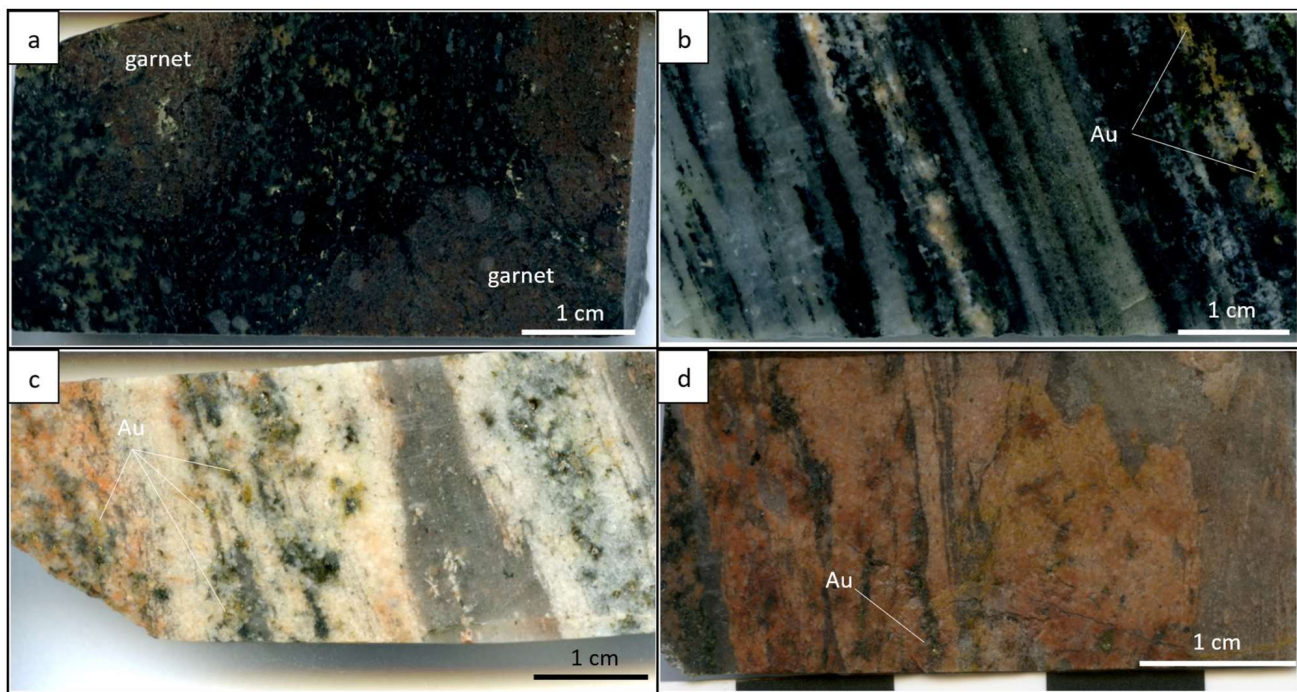


Figure 3. Images of samples selected for mineral geochemistry and P - T work including: (a) garnet-bearing amphibolite at ~800m north of Tick Hill pit (sample TH99); (b) gold-bearing, amphibole-rich calc-silicate (sample TH46); and (c, d) quartz-feldspar mylonite (samples TH55, THM22, respectively).

Table 1. List of samples and minerals pairs geochemically analysed for barometry (P) and thermometry (T) estimates.

Tectonic event	Sample	Rock type	Mineral (pairs) of geothermobarometry	Zone 54-GDA	
				East (m)	North (m)
D ₁₋₂	TH99	Amphibolite	Garnet-plagioclase-hornblende-quartz (P); hornblende-plagioclase (T); garnet-biotite (T)	389 017	7 606 713
D ₁₋₂	TH46	Amphibole-rich calc-silicate	Hornblende-plagioclase (T)	388 849	7 605 927
D ₃	TH55	Quartz-feldspar mylonite	Chlorite (T)	388 834	7 605 923
D ₃	THM22	Quartz-feldspar mylonite	Chlorite (T)	388 850	7 605 947

gneiss, amphibole-rich calc-silicate (*i.e.* amphibole-bearing and amphibole-chlorite-epidote-bearing calc silicates) and quartz-feldspar mylonite (a variety of so-called 'galahstone'), which formed under peak-metamorphic conditions (Figure 3a-d; Le *et al.*, 2021a, 2021b). The amphibole gneiss is commonly intercalated with the calc-silicate unit in and around the Tick Hill mining pit, whereas the amphibole-rich calc-silicate and quartz-feldspar mylonite, together with biotite-rich schist, are sub-units of the biotite-schist-dominated unit that occurs in the central part of the deposit (Le *et al.*, 2021a).

Four samples were selected for major-element mineral analyses (Table 1). Two samples contain D₁₋₂ peak-metamorphic mineral assemblages (samples TH46 and TH99), whereas the other two samples contain D₃ hydrothermal mineral assemblages (samples TH55 and THM22).

Sample TH99 was collected from the amphibolite gneiss in the drill core at ~800m north of Tick Hill pit (Figure 3a). It

contains coarse-grained garnet, intergrown hornblende-biotite-plagioclase-quartz-apatite-ilmenite-magnetite, and pyrite and chalcopyrite (Le *et al.*, 2021a). The granoblastic garnet (Figure 3a) is coarse-grained (1-3 cm diameter) and contains inclusion trails of hornblende, quartz and ilmenite, with minor apatite, biotite (*e.g.* Figure 4a-d), pyrite and chalcopyrite. Hornblende is commonly coarse-grained, granoblastic and aligned in the S₁₋₂ fabric (Figure 4a, b), and coexists with plagioclase, quartz and garnet. Plagioclase is found in contact with hornblende, quartz and garnet. Biotite only occurs as inclusions within garnet. The garnet-biotite-hornblende-plagioclase-quartz assemblage can be used to constrain the early D₁ P - T conditions, using the garnet-plagioclase-hornblende-quartz barometer and hornblende-plagioclase, garnet-hornblende and garnet-biotite thermometers (Ferry & Spear, 1978; Hodges & Spear, 1982; Holland & Blundy, 1994; Kohn & Spear, 1990). The amphibolite is locally cut by D₃ micro-veins of chalcopyrite-chlorite, but the peak-metamorphic minerals selected for geothermobarometry are not affected by D₃.

Sample TH46 comes from a granoblastic amphibole-rich calc-silicate unit within the ore zone and was collected from drill core. The rock has a mineral assemblage of diopside-scapolite-hornblende-actinolite-plagioclase-quartz with alternating domains of hornblende-diopside, and plagioclase-scapolite-quartz defining a gneissic S₁₋₂ fabric (*e.g.* Figure 5a, b). The hornblende-plagioclase pairs that were used to determine the formation temperature of this D₁ mineral assemblage form part of the same equilibrium assemblage (Figure 5c). The sample is gold-rich and has a strongly developed S₁₋₂ fabric overprinted by D₃ hydrothermal alteration. The gold inclusions are hosted in hornblende, diopside and scapolite, and occur in two forms (Figures 3b and 5b, d): (1) as fine inclusions concentrated along

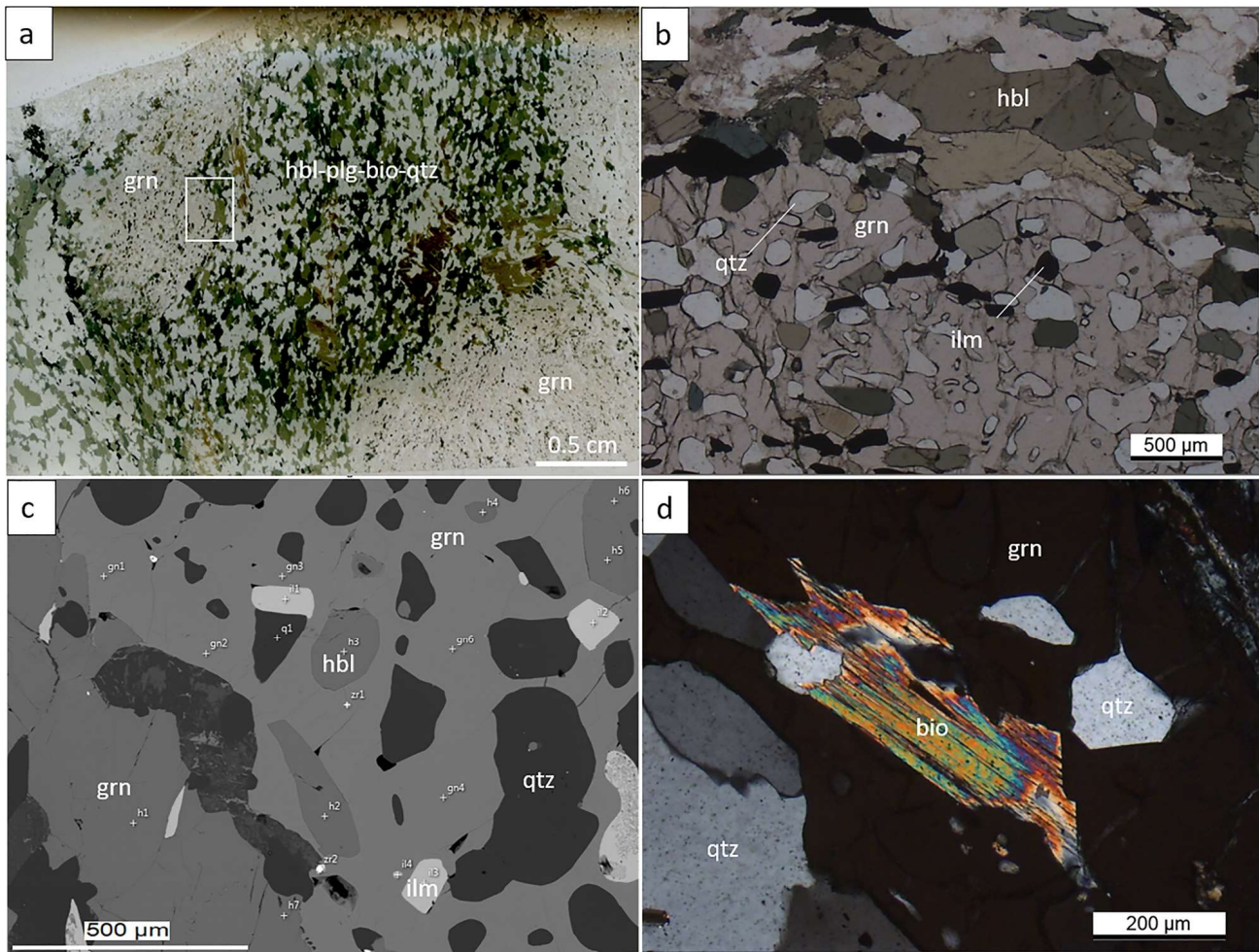


Figure 4. Representative images of D_{1-2} assemblages for sample TH99 from the amphibole gneiss unit. (a) Scanned image of polished thin-section showing coarse grain of garnets (grn) associated with hornblende–plagioclase–biotite–quartz (hbl–plg–bio–qtz), in which the hornblende and biotite are aligned with the S_1 fabric. The white box area is enlarged in (b). (b) Granoblastic hornblende (hbl) aligned in S_{1-2} , bounding a large garnet grain (grn) with inclusions of hornblende, quartz (qtz) and ilmenite (ilm) under plane-polarised light. (c) SEM image showing inclusions of quartz (qtz), hornblende (hbl) and ilmenite (il) inside a garnet grain. (d) Biotite (bio) and quartz (qtz) inclusions in garnet (grn) under cross-polarised light.

micro-fractures of hornblende and diopside, and (2) as fine- to coarse-grained inclusions contained within compositionally homogeneous hornblende, diopside and scapolite with no evidence of micro-fracturing. The fact that gold inclusions occur in hornblende, which itself occurs as an inclusion in diopside and scapolite (Figure 5d), indicates that gold was present during growth of the peak-metamorphic assemblage (Le *et al.*, 2021a). Actinolite locally replaces hornblende, including those that contain gold inclusions. The late (*i.e.* D_3) gold accumulation is also commonly recorded in this rock type and occurs in micro-veins in hornblende or as fine grains associated with altered hornblende around D_1 coarse-grained gold. These fine gold grains were interpreted as remobilised gold (Figure 5b; Le *et al.*, 2021a).

The last two samples, TH55 and THM22, were collected from the Au-rich zone of the mylonite unit (Figure 3c, d) from drill core (TH55) and the mining pit (THM22). These samples contain D_3 actinolite–chlorite–epidote–albite–K-feldspar–hematite–calcite alteration assemblages. Chlorite alteration shows a gradual shift in morphology from chlorite₁ (after biotite) to chlorite₂ (after chlorite₁; Le *et al.*, 2021a). Chlorite₁ formed during stage 2 and

pseudomorphed peak-metamorphic biotite (*e.g.* Figure 6a, b; Le *et al.*, 2021a). Chlorite₂ replaced chlorite₁ during stage 3, which is one of two main stages during which gold was remobilised, and commonly contains fine gold inclusions (Figure 6c; Le *et al.*, 2021a). Chlorite₂ commonly shows complex textures with irregular shapes (*e.g.* forming reaction-rims around earlier sulfides; Figure 6b). Chlorite₃ formed during stage 4 and is intergrown with calcite (Figure 6d; Le *et al.*, 2021a). It occurs only in small amounts compared with chlorite₂. The chlorite₁₋₃ compositions were used to constrain the D_3 mineralisation temperatures.

Methodology

All mineral chemistry analyses were undertaken at the Advanced Analytical Centre, James Cook University (JCU), using a Jeol JXA-8200 superprobe with a wavelength-dispersive spectrometer. The thin-sections were carbon-coated to increase the conductivity of the samples before analysis. A focus beam (<1 μm) at an accelerating voltage of 20 kV and a beam current of 20 nA was used. The details of this technique are presented in

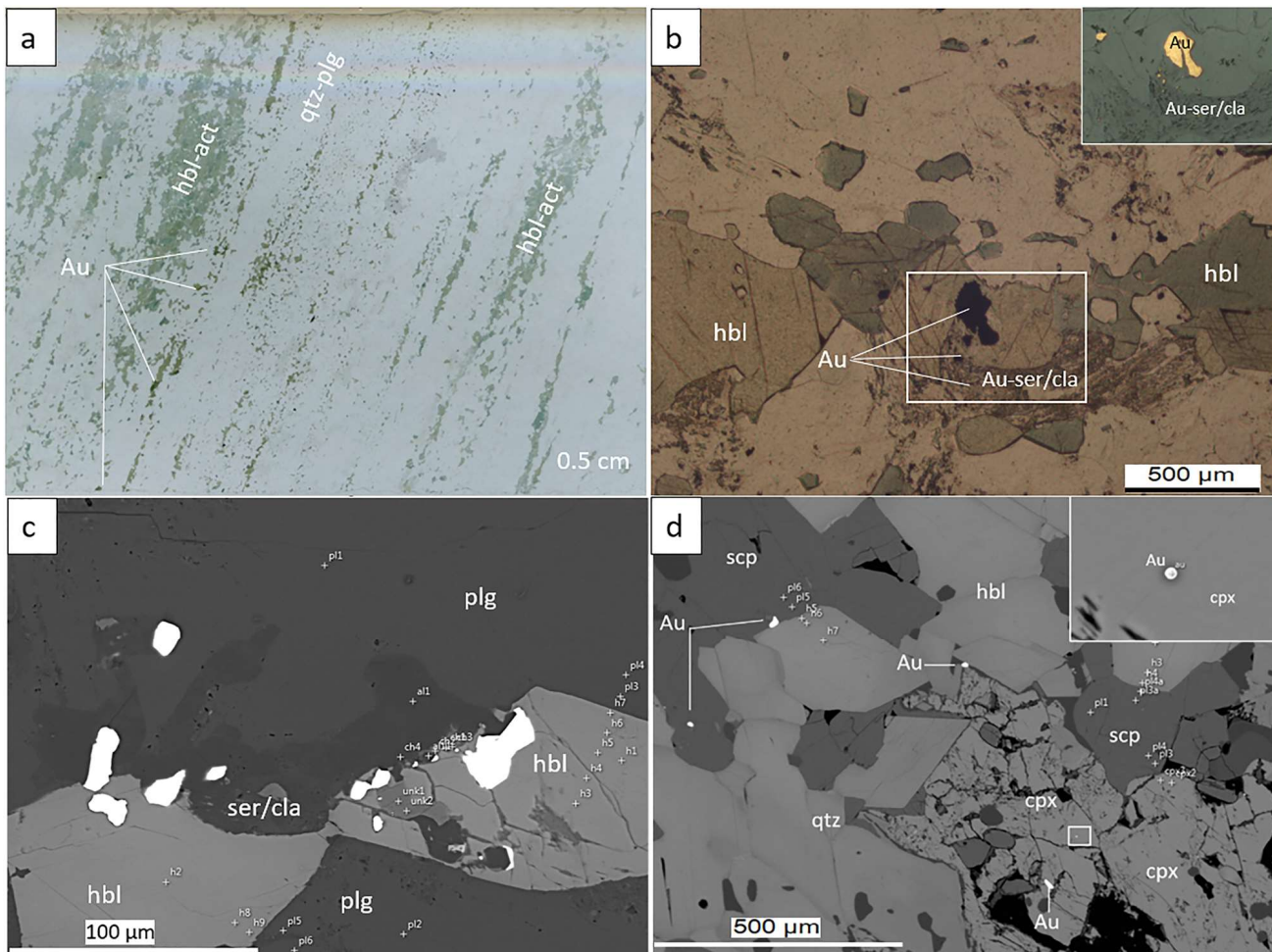


Figure 5. Representative images of D_{1-2} assemblages for sample TH46 from the amphibolite calc-silicate unit. (a) Scanned image of the polished thin-section showing amphibole-rich calc-silicate including hornblende–actinolite (hbl–act) intercalated with quartz–plagioclase (qtz–plg) that aligned with the S_1 fabric (Le *et al.*, 2021a). (b) Weakly foliated D_{1-2} Au-bearing hornblende (hbl) in amphibole-rich calc-silicate overprinted by D_3 hydrothermal events that caused fine-grained gold to remobilise along grain boundaries (inserted image from the white box) where it is associated with sericite (ser) and clay (cla) alteration. (c) Diopside grain (cpx, marked by irregular white line) containing Au (inset from the white box) and actinolite inclusion (act), which appears to occur with hornblende (hbl) during D_{1-2} event and is overprinted by D_3 hydrothermal events that are evidenced by sericite and clay (ser/clo) alteration. (d) SEM images of gold (Au) inclusions in scapolite (scp) and diopside (cpx) in amphibole-rich calc-silicate, sample TH46. The area enclosed in the white box is enlarged in the insert and shows a gold inclusion in clean diopside.

Jercinovic *et al.* (2008). The output data, expressed in weight percentages, were used to calculate the mineral formulas for feldspar, garnet, amphibole, pyroxene, biotite and chlorite. The Fe^{3+} contents from garnet, amphibole and chlorite are calculated based on formulas of Droop (1987), Ridolfi *et al.* (2018) and Yavuz *et al.* (2015), respectively. The methods for garnet–plagioclase–hornblende–quartz barometry and hornblende–plagioclase, garnet–biotite, garnet–hornblende and chlorite thermometry are presented in following sections. Core and rim analyses were carried out for testing for compositional homogeneity. Spear and Kohn (1999) have written a program named GTB, which compiles calibrations for a wide range of classical geothermobarometers that can be applied to a range of bulk compositions. The latest version of GTB (provided in 2021 by the author, Prof. Frank Spear) has been used for all P – T estimates in this study, except for temperature estimates obtained from chlorite, for which the calibrations of Cathelineau (1988) and Jowett (1991) were used.

Results

The major-element compositions of mineral pairs (*i.e.* garnet–plagioclase–hornblende–quartz, plagioclase–hornblende, garnet–biotite) were obtained from the clean margin area of each mineral (Figure 7) for the barometric and thermometric estimation, except for quartz that is always present as 100% SiO_2 . For the chlorite thermometry, the major-element analyses were typically obtained from a range of spots cutting across the chlorite flakes or at the cleanest domains of chlorite in the flake (Figure 8).

Garnet–plagioclase–hornblende–quartz barometry (sample TH99)

The garnet–plagioclase–hornblende–quartz barometer was developed by Kohn and Spear (1989), revised by Kohn and Spear (1990) and applied to metamorphic rocks including amphibolite. The technique calibrations using tschermakite (*i.e.* Fe–Mg)

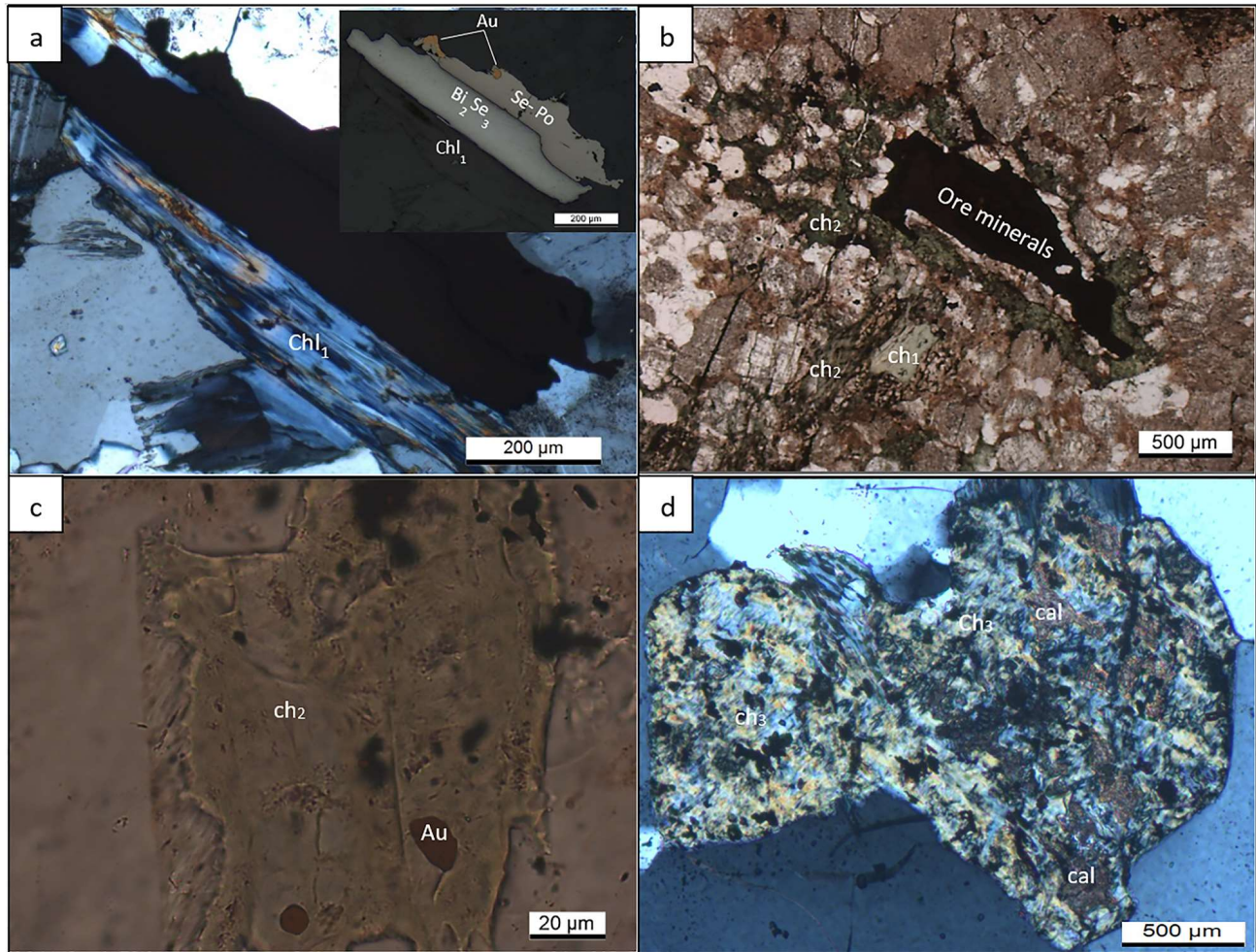


Figure 6. Photomicrographs showing D_2 alteration minerals in various quartz–feldspar mylonite units in the most strongly altered core of the ore zone. (a) Early D_3 chlorite₁ (ch_1) with morphology of initial mineral of biotite (Le *et al.*, 2021a) and associated with bismuth selenide (Bi_2Se_3), selenide-rich pyrrhotite (Se–Po) and gold (sample TH55), with an inserted image captured from reflected light. (b) Chlorite₂ (ch_2) replacing chlorite₁ (ch_1 , Le *et al.*, 2021a) and occurring around an ore mineral (pyrite–chalcopyrite intergrowth) as a reaction rim (sample THM22). (c) Chlorite₂ (ch_2) hosting inclusions of gold (sample TH55). (d) Chlorite₃ (ch_3) intergrown with calcite (cal; sample TH55).

exchange reactions for the same mineral assemblage in amphibole have an estimated uncertainty of 0.5–1 kbar (Kohn & Spear, 1990). The peak-metamorphic amphibole in sample TH99 has a near-identical composition and mineral assemblage to those used for the pressure estimates in both calibrations. Thus, the calibration of Kohn and Spear (1990) using the tschermakite exchange reaction was applied to estimate P for the D_{1-2} peak-metamorphic conditions. The compositions of garnet–plagioclase–hornblende groups used for barometry are presented in Table 2. Representative minerals pairs and analyses are shown in Figure 7a, with the results of the pressure estimates shown in Figure 9a. The Mg-endmember model yielded pressure estimates of 6–7 kbar that are largely independent from T , whereas the Fe-endmember model yielded temperature-dependent pressure estimates of 6–8 kbar in the temperature range of 600–800 °C.

Hornblende–plagioclase thermometry (samples TH46 and TH99)

The hornblende–plagioclase Fe–Mg exchange geothermometer was developed by Spear (1980, 1981), based on

hornblende–plagioclase pairs in metamorphic rocks, and has since then been reviewed by Essene (1989), Spear (1993) and Anderson (1996). In addition, Blundy and Holland (1990) formulated a calibration for the equilibrium reaction ‘edenite + 4 quartz = tremolite + albite’, based on experimental and empirical data, to account for non-ideal mixing in plagioclase, but this calibration was criticised by Poli and Schmidt (1992) for its imprecision. Holland and Blundy (1994) generated a revised calibration for the same equilibrium reaction (model A) and suggested that it should be applied to hornblende–plagioclase assemblages in quartz-bearing amphibolites. Holland and Blundy (1994) also formulated a new calibration for the equilibrium reaction ‘edenite + albite = richterite + anorthite’ (model B) for hornblende–plagioclase assemblages in non-quartz-bearing amphibolites. The model A calibration was used in this study, because all selected samples from Tick Hill contain quartz.

Hornblende–plagioclase temperature estimates for sample TH99

The composition of hornblende–plagioclase pairs used for temperature estimates is shown in Table 3, and representative

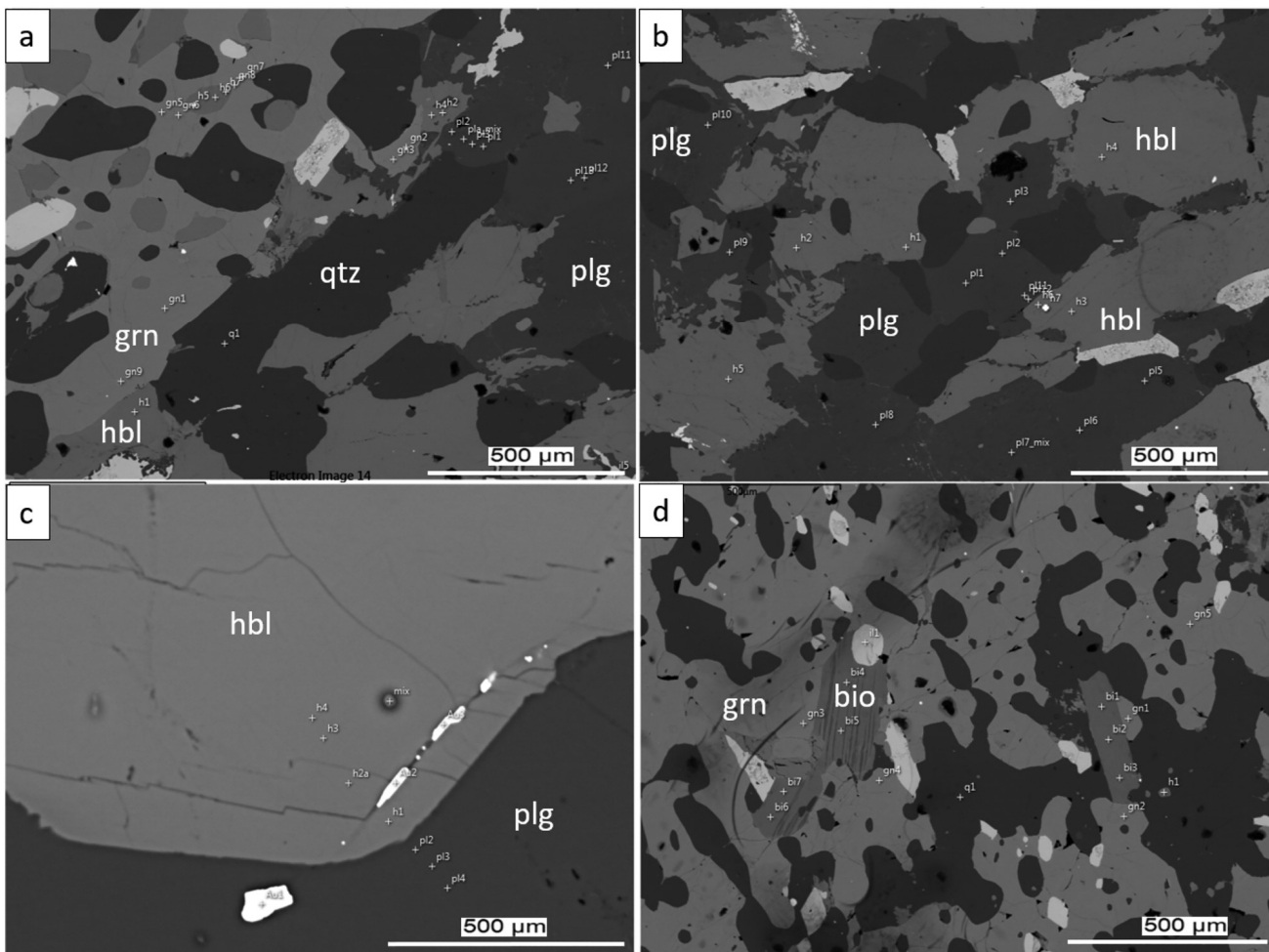


Figure 7. Representative SEM images of geobarometry analyses. (a) Garnet–hornblende–plagioclase–quartz (grn–hbl–plg–qtz) barometry for sample TH99 from amphibole gneiss. (b) Plagioclase–hornblende (plg–hbl) thermometry for sample TH99. (c) Plagioclase–hornblende (plg–hbl) thermometry for sample TH46 from the amphibole-rich calc-silicate unit. (d) Garnet–biotite (grn–bio) thermometry for sample TH99 from amphibole gneiss.

minerals pairs and analyses are shown in [Figure 7b](#). The results of temperature estimates for hornblende–plagioclase pairs, using Holland and Blundy (1994), are shown in [Figure 9a](#). Temperature estimates, based on model A calibrations, yielded temperatures of 700–750°C over a wide range of pressures. Using the pressure estimates from the garnet–plagioclase–hornblende–quartz barometer discussed above as an input, the preferred P – T range for the formation of amphibolite gneiss is the intersection domain between the pressure estimate lines and temperature lines, which are 720–750°C and 6.0–7.6 kbar ([Figure 9a](#)).

Hornblende–plagioclase temperature estimates for sample TH46

The compositions of the hornblende–plagioclase pairs for this sample are shown in [Table 3](#), and representative minerals pairs and analyses are shown in [Figure 7c](#). Note that some analyses were conducted near the micro-veins of gold inside D_1 hornblende, and this gold could be the result of D_{1-2} retrograde or D_3 mineralisation (Le *et al.*, 2021a). The P – T estimates calculated

using Holland and Blundy (1994) models are shown in [Figure 9b](#). Using the pressure estimates obtained from TH99, the preferred temperature range for the formation of this mineral pair is 620–670°C.

Garnet–biotite thermometry (sample TH99)

Numerous calibrations for the garnet–biotite Fe–Mg exchange geothermometer are available (e.g. Berman, 1990; Ferry & Spear, 1978; Hodges & Spear, 1982; Perchuk & Lavrent'eva, 1983; Thompson, 1976). Many of these calibrations consider not only the concentration of Fe and Mg in garnet and texturally corresponding biotite, but also the influence of the Ca and Mn content in garnet and Ti and Al^{IV} content in biotite. The first experimental calibration was conducted by Ferry and Spear (1978) using the quartz–fayalite–magnetite oxygen fugacity buffer at 2.07 kbar in a simple KFMASH system with biotite with a low Al content. Hodges and Spear (1982) presented an alternative calibration by combining the solution models for garnet presented by Ganguly and Kennedy (1974) and Newton *et al.* (1977), and the revised Ferry and Spear (1978) calibration with the assumption of ideal mixing in biotite. This calibration was

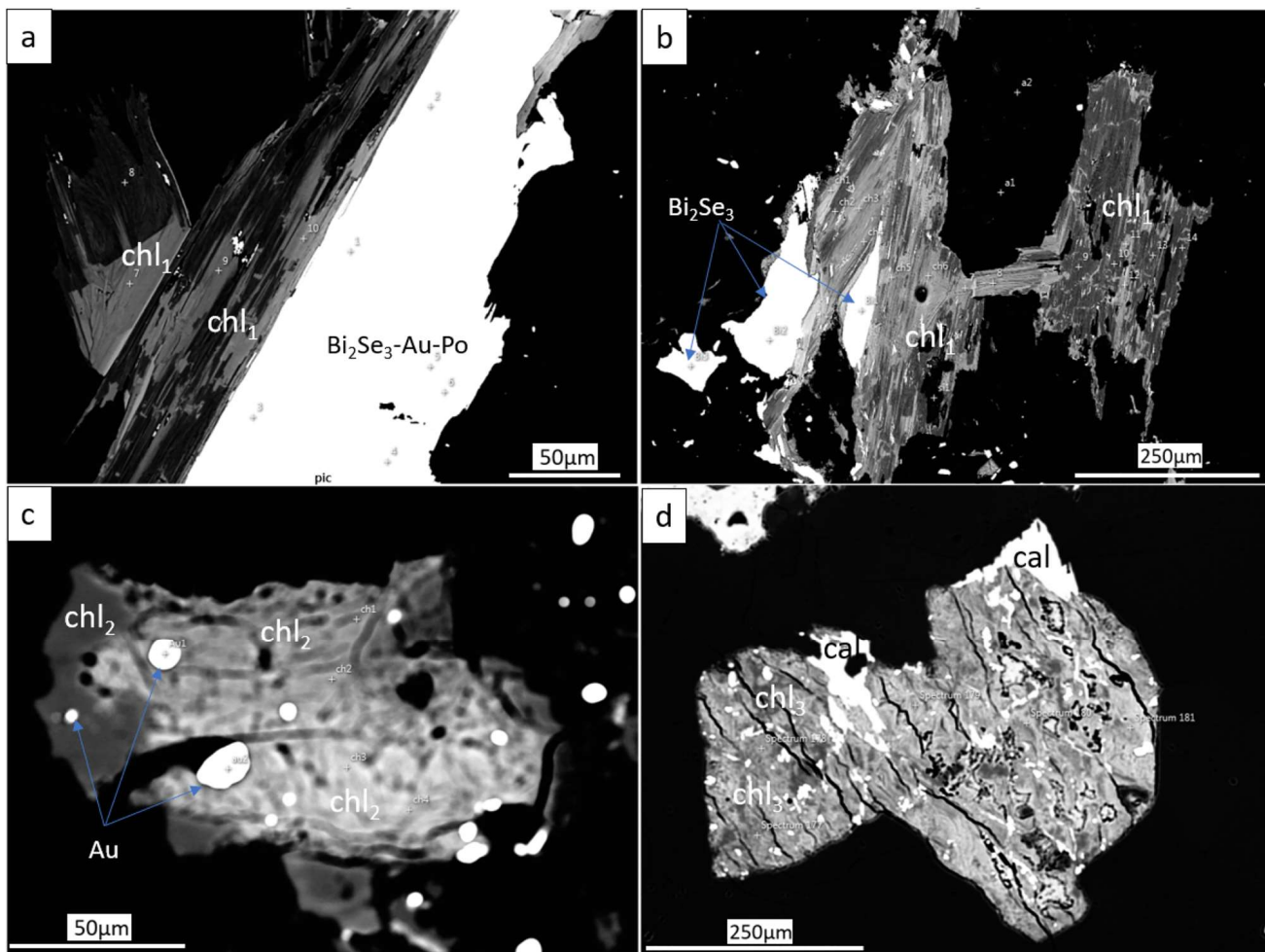


Figure 8. Representative SEM images of chlorite thermometry analyses for Au-rich quartz–feldspar mylonite, sample TH55. (a, b) Chlorite, (chl₁) that is altered from biotite and associated with bismuth selenide (\pm Au, pyrrhotite) in Au-rich quartz–feldspar mylonite, sample TH55. (c) Chlorite₂ (chl₂) containing inclusions of gold (Au). (d) Chlorite₃ (chl₃) associated with calcite.

based on metapelitic rocks and resulted in an estimated error range of ± 15 – 25 °C. Perchuk and Lavrent'eva (1983) generated a new experimental calibration using the Ni–NiO oxygen fugacity buffer at 6 kbar, natural garnet and high-Al biotite from metapelite but ignored the problem of non-ideal mixing in natural minerals. Berman (1990) developed a garnet–biotite thermometry that accounts for Ti and Al in biotite using a linear programming method, and he incorporated most of the available qualified experimental and natural data at time, excluding data from Perchuk and Lavrent'eva (1983).

The compositions of the garnet–biotite pairs for sample TH99 are shown in Table 4. Representative minerals pairs and analyses are shown in Figure 7d. Temperature estimates for biotite–garnet pairs in TH99 using the GTB program are presented in Figure 9c, noting that most garnet–biotite calibrations are based on pelitic bulk compositions, and the garnet–biotite thermometer is susceptible to retrograde re-equilibration. Four calibration models (Berman, 1990; Ferry & Spear, 1978; Hodges & Spear, 1982; Perchuk & Lavrent'eva, 1983) were selected for the garnet–biotite T calculations. Assuming a preferred pressure range of 6.0–7.6 kbar from the garnet–plagioclase–hornblende–quartz barometer, the Perchuk and Lavrent'eva (1983) and Ferry

and Spear (1978) calibration yield temperature estimates of 625–655 °C and 670–715 °C, respectively, while the Hodges and Spear (1982) and Berman (1990) calibrations provide temperature estimates of 717–760 °C and 725–770 °C, respectively. The latter estimates are consistent with the hornblende–plagioclase temperature estimates (Figure 9a).

Garnet–hornblende thermometry (sample TH99)

Garnet–hornblende Fe–Mg exchange geothermometers have been developed for over 40 years (e.g. Graham & Powell, 1984; Perchuk *et al.*, 1985; Powell, 1985; Ravna, 2000). Graham and Powell (1984)'s semi-empirical garnet–hornblende geothermometer used Fe–Mg exchange between garnet and hornblende from Ellis and Green (1979) that has been widely applied for their early calibrations. This thermometer is applicable to hornblende-rich metamorphic rocks containing Mn-poor garnet that are interpreted to have formed at a low oxygen fugacity below 850 °C and can also be applied to metagreywacke and mafic schist (Graham & Powell, 1984). Perchuk *et al.* (1985) presented a new graph-based amphibole–garnet thermometry based on the modification of his earlier isotherms in Perchuk

Table 2. Compositions of garnet–plagioclase–amphibole pairs from amphibolite (sample TH99) used for pressure estimates.

	Sample	TH99-P1	TH99-P2
Garnet	SiO ₂	37.82	37.82
	Al ₂ O ₃	20.19	20.18
	FeO _T	31.57	30.45
	MnO	1.69	1.67
	MgO	3.58	3.76
	CaO	4.80	4.77
	Sum	99.65	98.65
	Si	3.03	3.05
	Al	1.90	1.92
	Fe ³⁺	0.04	0.00
	Fe ²⁺	2.08	2.07
	Mn	0.11	0.11
	Mg	0.43	0.45
	Ca	0.41	0.41
	Almandine	68.53	67.96
	Spessartine	3.78	3.74
	Pyrope	14.10	14.80
Plagioclase	Grossular	13.33	13.65
	Ab	58.76	57.95
	An	40.91	40.34
Amphibole	Or	0.32	1.71
	SiO ₂	39.86	39.92
	TiO ₂	0.82	0.90
	Al ₂ O ₃	14.67	14.65
	FeO	20.87	21.59
	MnO	0.14	0.14
	MgO	6.64	6.76
	CaO	10.50	10.55
	Na ₂ O	1.91	1.92
	K ₂ O	0.77	0.80
	Cl	1.18	1.16
	Sum	97.37	98.40
	Si	6.08	6.03
	Ti	0.09	0.10
	Al ^{iv}	1.92	1.97
	Al ^{vi}	0.72	0.63
	Fe ³⁺	0.87	1.01
Fe ²⁺	1.79	1.72	
Mn	0.02	0.02	
Mg	1.51	1.52	
Ca	1.72	1.71	
Na	0.56	0.56	
K	0.15	0.15	
Cl	0.30	0.30	

(1967, 1969, 1970). More recently, Thomas and Rana (2020) applied three early models (Graham & Powell, 1984; Perchuk *et al.*, 1985; Powell, 1985) and a later model developed by Ravna (2000) to 79 samples collected from different metamorphic rocks and concluded that the calibration of Perchuk *et al.* (1985) is the most reliable for a wide range of greenschist to eclogite facies metamorphic rocks. The garnet–hornblende calibrations of Perchuk *et al.* (1985) and Graham and Powell (1984) were therefore used for sample TH99. As with other geobarometry estimates in this study, the calculation was completed using the updated 2021 version of Spear and Kohn (1999)'s GTB program.

Three garnet–hornblende pairs from Sample TH99 were selected for the thermometric study (Table 5; Figure 7d). The temperature estimates used the Perchuk *et al.* (1985) calibration and yielded a temperature range of 590–615 °C, while temperature estimates using Graham and Powell (1984)'s calibration yielded a temperature range of 565–585 °C (Figure 9d). These temperature estimates are independent of pressure and are significantly lower than the temperature estimates derived from the hornblende–plagioclase and biotite–garnet thermometers (Figure 9a).

Chlorite thermometry

Chlorite thermometry has been used in the study of alteration assemblages to constrain the temperature of mineralising fluids (Essene, 2009). The chlorite empirical thermometer was first formulated by Cathelineau and Nieva (1985) and then revised by Cathelineau (1988) and Jowett (1991). Details of chlorite thermometers have been presented in various reviews (*e.g.* Bourdelle & Cathelineau, 2015; Essene, 2009; Inoue *et al.*, 2009; Vidal *et al.*, 2016). In general, Cathelineau and Nieva (1985) used the variation in Al^{iv} contents (based on 28 oxygen per formula unit) in chlorite as a function of temperature, which was subsequently revised by Cathelineau (1988) by reselecting chlorite flake samples for the experiment:

$$T^{\circ}\text{C} = -61.92 + 321.89 \text{Al}^{\text{iv}}$$

Jowett (1991) used the Al^{iv} contents (based on 14 oxygen formula) of chlorite in combination with an Fe / (Fe + Mg) correction to reflect variations owing to bulk composition and mineral reactions at changing conditions, and created a *T*–Al relationship:

$$T^{\circ}\text{C} = 318.5[\text{Al}^{\text{iv}} + 0.1(\text{Fe} / (\text{Fe} + \text{Mg}))] - 68.7$$

The empirical chlorite thermometers are still widely used in ore-deposit alteration studies in low-grade rocks (*e.g.* Esteban *et al.*, 2007; Gillis *et al.*, 2001; Laverne *et al.*, 1995; Moura *et al.*, 2006; Timpa *et al.*, 2005; Zang & Fyfe, 1995), despite being criticised for their reliability (*e.g.* Essene, 2009; Essene & Peacor, 1995) or their applicability to metamorphic rocks (Vidal *et al.*, 2006). In this study, the chlorite thermometers of Cathelineau (1988) and Jowett (1991) have been applied to constrain the temperature ranges over which D₃ hydrothermal mineralisation events took place.

The composition of chlorite and the temperature estimates are shown in the supplemental data (Table S1). As mentioned earlier, chlorite compositions and textures indicated three chlorite types (chlorite₁ to chlorite₃). Representative analyses for these chlorites are shown in Figure 8. Chlorite₁ and chlorite₃ have the highest and lowest Al₂O₃ contents, respectively. The temperature estimates, using the Jowett (1991) and Cathelineau (1988) calibrations, are shown in Figure 10a and b, respectively. The estimated $T_{\text{Jowett (1991)}}$ is 280–385 °C for chlorite₁, 160–270 °C for chlorite₂ and 130–170 °C for chlorite₃. The estimated $T_{\text{Cathelineau (1988)}}$ is 3–8 °C lower than $T_{\text{Jowett (1991)}}$ for all three chlorite types. Collectively, the chlorite results show a near-continuous temperature range of 130–380 °C, reflecting retrograde re-equilibration as the various stages of D₃ alteration progressed.

Discussion

P–*T* estimates for peak-metamorphic amphibolite

The geothermobarometry study for peak-metamorphic amphibolite is based on pressure estimates for the garnet–plagioclase–hornblende–quartz assemblage and temperature estimates for hornblende–plagioclase, garnet–hornblende and garnet–biotite assemblages. The pressure range is defined by the

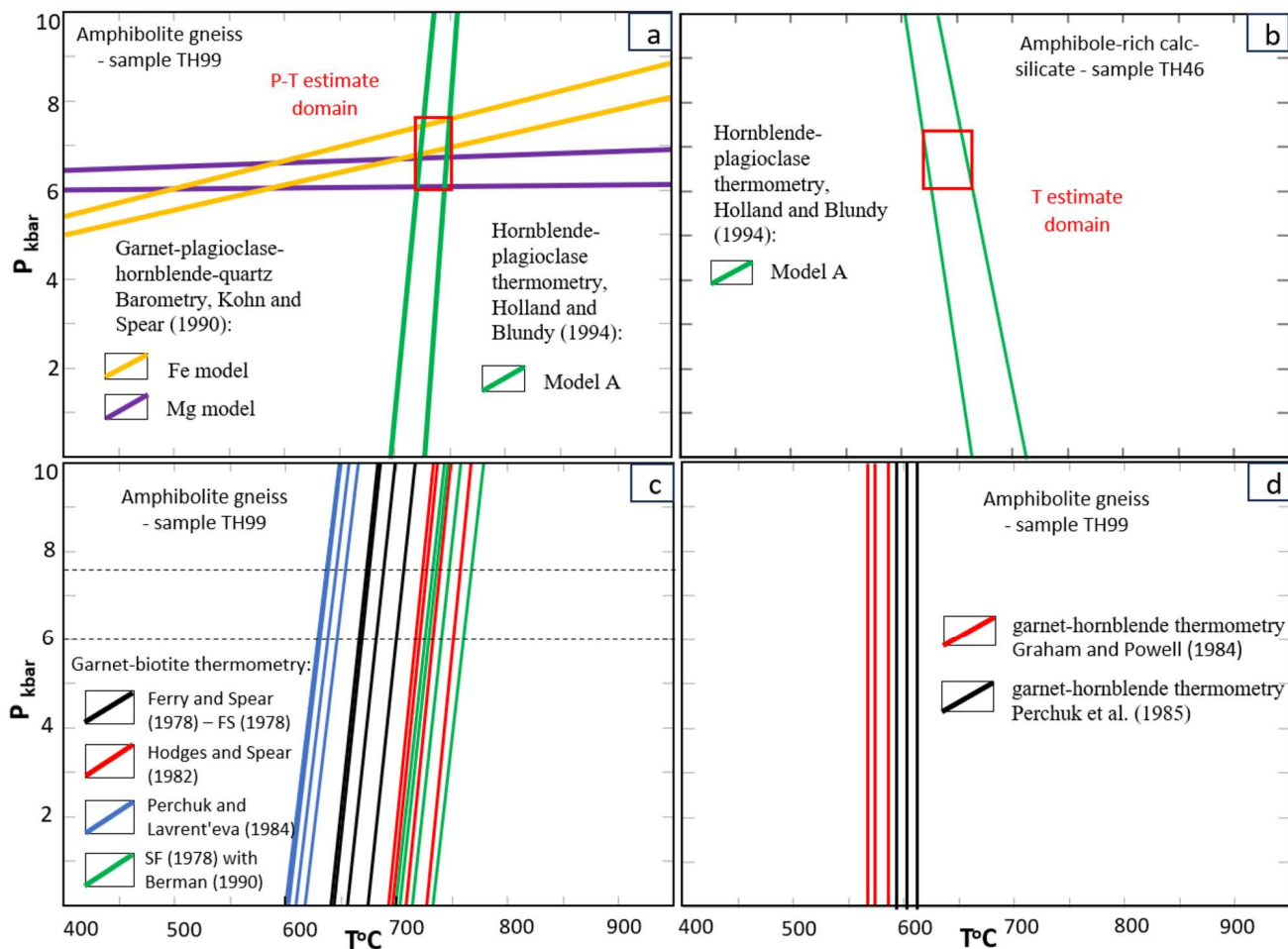


Figure 9. Geobarothermometry results for mineral assemblages and chlorites at the Tick Hill Area. (a) Garnet–plagioclase–hornblende–quartz pressure estimates (after Kohn & Spear, 1990) and hornblende–plagioclase temperature estimates (after Holland & Blundy, 1994) for peak metamorphic (D_{1-2}) assemblages in amphibole gneiss unit (sample TH99). The P – T estimates are defined by the overlap region of the thermometer and barometer that is 6.0–7.6 kbar at 720–750 °C (model A). (b) Hornblende–plagioclase temperature estimates for the mineralised amphibole-rich calc-silicate unit (sample TH46) using Holland and Blundy’s (1994) (models A) thermometers. The T estimate is defined by the overlap region of the two model that is 620–670 °C. (c) Temperature estimates based on the garnet–biotite Fe–Mg-exchange geothermometer using calibrations of Ferry and Spear (1978), Hodges and Spear (1982), Perchuk and Lavrent’eva (1983) and Berman (1990) for sample TH99. (d) Garnet–hornblende thermometry results for amphibole gneiss unit (sample TH99) calculated from calibration of Graham and Powell (1984) and Perchuk *et al.* (1985).

garnet–tschermakite–plagioclase–quartz barometry for the amphibolite gneiss (sample TH99) using Kohn and Spear (1990) calibrations and is estimated to be 6–7.6 kbar (Figure 9a). Using this pressure range as an input for the Holland and Blundy (1994) hornblende–plagioclase thermometry diagram, the temperature estimates are 720–750 °C (model A; suggested for the quartz-bearing amphibolite) and 730–780 °C (model B; suggested for the non-quartz-bearing amphibolite) (Figure 9a). Because the typical mineral assemblage for the amphibolite gneiss (sample TH99) is garnet–tschermakite–plagioclase–quartz, the estimated temperature range of 720–750 °C from Holland and Blundy (1994)’s hornblende–plagioclase (model A) calibration is preferred in this study. Thus, the estimated P – T range for rocks in the Tick Hill area during D_1 is 6.0–7.6 kbar and 720–750 °C (Figure 9a). This high temperature of formation is compatible with the observed migmatization in the surrounding gneiss (Le *et al.*, 2021a). The obtained temperature range from the hornblende–plagioclase thermometry is comparable with the garnet–biotite pairs using the calibrations of Hodges and Spear (1982) and Berman (1990),

which are 717–760 °C and 725–770 °C, respectively. The garnet–hornblende temperature estimates based on Graham and Powell (1984) and Perchuk *et al.* (1985) are 565–585 °C and 590–615 °C, respectively, 100–150 °C lower than other estimates (Figure 9d). Considering that sample TH99 shows little compositional variation in any of the mineral phases for the different grains and from rim to core (Tables 2–5) and does not show any evidence for significant retrograde alteration or re-equilibration, it is possible that there is some disequilibrium between the garnet and hornblende. In this case, garnet possibly grew syn- to late hornblende crystallisation, which is reflected in their compositions as well as the temperature estimates.

The gneissic and migmatization textures and P – T estimates (6–7.6 kbar, 720–750 °C), for the garnet-bearing amphibolite gneiss ~800 m north of Tick Hill, indicate that high-grade metamorphism is only locally preserved in the area. In most places in and around the Tick Hill pit, peak-metamorphic assemblages are largely re-equilibrated and destroyed during later retrograde metamorphism and hydrothermal alteration.

On a broader scale (*i.e.* in Mary Kathleen Domain and Mount Isa Province), the rocks have been affected by four distinct metamorphic–magmatic events, including (1) the 1870–1840 Ma Barramundi Orogeny (Betts *et al.*, 2016; Blake & Steward, 1992), (2) the 1790–1770 Ma metamorphism and magmatism in the Tick Hill region (Le *et al.*, 2021b) that has not been linked to a specific regional event, (3) the 1740–1720 Ma Wonga Orogeny (Spence *et al.*, 2021, 2022) and (4) the 1600–1500 Ma Isan

Orogeny (Le *et al.*, 2022; Oliver, 1995; Withnall & Hutton, 2013). The 1790–1770 Ma peak metamorphism conditions at amphibolite–granulite facies temperature and moderate pressure in the Tick Hill area have been higher than the other events listed above, which all experienced amphibolite facies metamorphic conditions at the northern Mary Kathleen and the Eastern Fold Belt (Oliver, 1995; Spence *et al.*, 2021, 2022; Withnall & Hutton, 2013).

Table 3. Hornblende–plagioclase compositions in amphibolite (sample TH99) and amphibole-rich calc-silicate (sample TH46) for temperature estimates.

Sample	TH99-T1	TH99-T2	TH46-T1	TH46-T2
Hornblende				
SiO ₂	39.93	40.01	48.50	48.77
TiO ₂	0.80	1.01	0.12	0.11
Al ₂ O ₃	14.62	14.44	6.93	6.84
FeO	20.87	20.88	14.97	13.88
MgO	6.71	6.90	13.79	13.87
MnO	0.18	0.16	0.15	0.16
CaO	10.21	10.32	11.59	11.57
Na ₂ O	1.92	1.87	1.50	1.35
K ₂ O	1.01	0.98	0.45	0.48
Cl	1.23	1.17	0.49	0.46
Sum	97.48	97.74	98.49	97.48
Si	6.08	6.07	7.01	7.10
Ti	0.09	0.12	0.01	0.01
Al ^{iv}	1.92	1.93	0.99	0.90
Al ^{vi}	0.70	0.65	0.19	0.27
Fe ³⁺	0.94	0.95	0.68	0.53
Fe ²⁺	1.72	1.70	1.13	1.16
Mn	0.02	0.02	0.02	0.02
Mg	1.52	1.56	2.97	3.01
Ca	1.67	1.68	1.79	1.80
Na	0.57	0.55	0.42	0.38
K	0.20	0.19	0.08	0.09
Cl	0.32	0.30	0.12	0.11
Plagioclase				
Ab	62.03	58.64	80.66	81.18
An	37.29	40.78	18.46	17.75
Or	0.67	0.59	0.88	1.07

Temperature estimates for D_{1–2} amphibole-rich calc-silicate and the distribution of gold

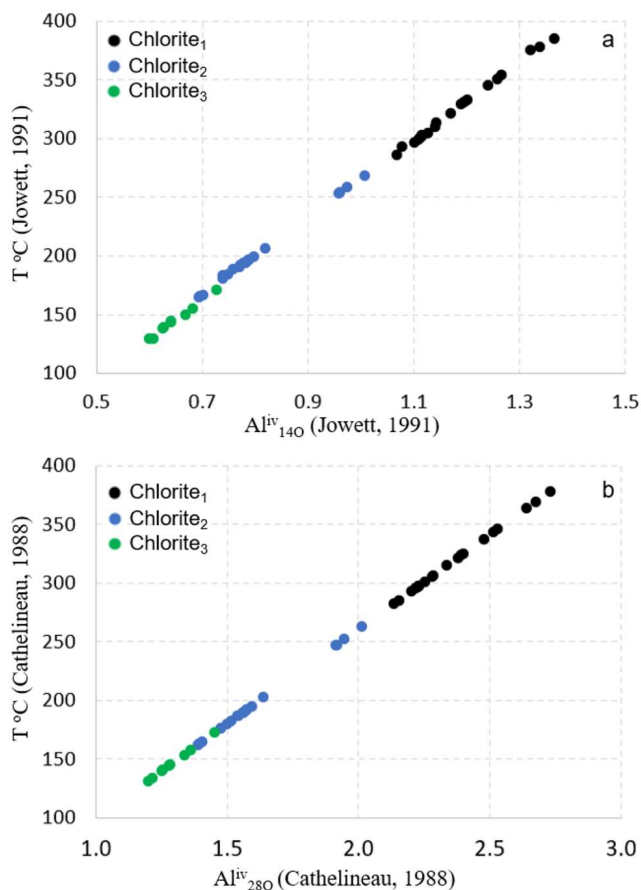
The temperature range for the gold-rich calc-silicate unit that preserves microstructural and mineralogical evidence for the D_{1–2} assemblage of diopside–hornblende–plagioclase and retrograde actinolite (Le *et al.*, 2021a) is 620–670 °C (Figure 9b). This temperature estimate is slightly lower, but comparable with that obtained from the garnet-bearing amphibolite gneiss (720–750 °C; sample TH99), which occurs only 800 m north of Tick Hill (Figure 2) and displays limited evidence for retrograde replacement or a hydrothermal overprint (Le *et al.*, 2021a). Although the diopside–hornblende assemblage in the calc-silicate sample is aligned with the dominant gneissic fabric, which is a composite D_{1–2} fabric, the lower temperature estimate suggests that this gold-bearing calc-silicate re-equilibrated during the later retrograde stages of the D_{1–2} events, or it was affected by the early D₃ overprint (Figure 5b). The fact that D₃ actinolite locally replaced hornblende (Le *et al.*, 2021a) is consistent with the suggestion of pervasive fluid infiltration during retrograde metamorphism, based on the narrow range of oxygen isotopic values [>+10.5 to +13.7‰ Vienna Standard Mean Ocean Water (VSMOW)] of quartz in different rock types that were reset during the D₃ regional fluid infiltration (Le *et al.*, 2022). Within this sample (*i.e.* TH46), gold occurs texturally in two distinct ways. It first occurs as inclusions within both

Table 4. Garnet–biotite compositions for amphibolite (sample TH99) for temperature estimates.

Sample	Garnet				Biotite			
	TH99_T11	TH99_T12	TH99_T13	TH99_T14	TH99_T11	TH99_T12	TH99_T13	TH99_T14
SiO ₂	37.75	37.75	37.75	37.80	36.25	33.99	35.21	34.68
TiO ₂	0.02	0.02	0.02	0.00	1.68	1.2174	1.6107	1.3668
Al ₂ O ₃	20.25	20.25	20.25	19.78	15.73	15.94	15.85	15.4
FeO	30.79	30.79	30.79	31.13	19.83	22.28	20.88	20.3
MnO	1.36	1.36	1.36	1.45	0.04	0.02	0.00	0.01
MgO	4.08	4.08	4.08	3.86	11.90	12.37	12.07	11.19
CaO	4.59	4.59	4.59	4.60	0.02	0.03	0.00	0.14
Na ₂ O	0.11	0.11	0.11	0.09	0.26	0.20	0.28	0.51
K ₂ O	0.03	0.03	0.03	0.02	8.49	6.27	7.72	7.79
Cl	0.01	0.01	0.01	0.01	1.10	0.81	0.98	1.14
Total	98.99	98.99	98.99	98.74	95.29	93.13	94.61	92.53
Si	3.03	3.03	3.03	3.05	5.52	5.35	5.43	5.50
Ti	0.00	0.00	0.00	0.00	0.19	0.14	0.19	0.16
Al ^{iv}	–	–	–	–	2.48	2.65	2.57	2.50
Al ^{vi}	–	–	–	–	0.34	0.31	0.31	0.38
Al	1.92	1.92	1.92	1.88	2.82	2.96	2.88	2.88
Fe ³⁺	0.01	0.01	0.01	0.01	–	–	–	–
Fe ²⁺	2.06	2.06	2.06	2.09	2.52	2.93	2.69	2.69
Mn	0.09	0.09	0.09	0.10	0.00	0.00	0.00	0.00
Mg	0.49	0.49	0.49	0.46	2.70	2.90	2.78	2.65
Ca	0.40	0.40	0.40	0.40	0.00	0.01	0.00	0.02
Na	–	–	–	–	0.08	0.06	0.08	0.16
K	0.00	0.00	0.00	0.00	1.65	1.26	1.52	1.58
Cl	0.00	0.00	0.00	0.00	0.28	0.22	0.26	0.31

Table 5. Garnet–amphibole compositions from amphibolite (sample TH99) for temperature estimates.

Sample	Garnet			Amphibole		
	TH99_T8	TH99_T9	TH99_T10	TH99_T8	TH99_T9	TH99_T10
SiO ₂	37.81	37.73	37.80	39.94	40.32	39.99
TiO ₂	0.00	0.00	0.00	1.07	1.17	0.83
Al ₂ O ₃	20.33	20.08	19.78	14.86	14.37	14.78
FeO	31.48	31.26	31.13	20.24	19.52	20.38
MnO	1.45	1.46	1.45	0.13	0.14	0.14
MgO	3.99	3.93	3.86	7.39	7.47	7.09
CaO	4.53	4.61	4.60	10.56	10.32	10.63
Na ₂ O	0.05	0.15	0.09	1.95	1.75	1.93
K ₂ O	0.03	0.04	0.02	1.01	1.13	0.91
Cl	0.00	0.01	0.01	1.27	1.22	1.35
Sum	99.68	99.26	98.74	98.42	97.40	98.04
Si	3.02	3.03	3.05	6.02	6.12	6.06
Ti	0.00	0.00	0.00	0.12	0.13	0.09
Al ^{iv}	–	–	–	1.98	1.88	1.94
Al ^{vi}	–	–	–	0.65	0.68	0.70
Al	1.91	1.90	1.88	2.64	2.57	2.64
Fe ³⁺	0.04	0.04	0.01	0.92	0.85	0.85
Fe ²⁺	2.06	2.06	2.09	1.63	1.63	1.73
Mn	0.10	0.10	0.10	0.02	0.02	0.02
Mg	0.48	0.47	0.46	1.66	1.69	1.60
Ca	0.39	0.40	0.40	1.70	1.68	1.73
Na	0.00	0.00	0.00	0.57	0.51	0.57
K	0.00	0.00	0.00	0.19	0.22	0.18
Cl	0.00	0.00	0.00	0.32	0.31	0.35

**Figure 10.** Temperature estimates for D₃ based on chlorite geothermometry using calibrations of (a) Jowett (1991) and (b) Cathelineau (1988) for chlorite alteration hosted in quartz–feldspar mylonite at Tick Hill (samples TH55 and THM22).

diopside and hornblende that are aligned in the gneissic fabric, which is consistent with similar observations reported by Choy (1994) and Tedman-Jones (2001). This gold occurs in parts of the metamorphic minerals that are homogeneous in composition and are not affected by visible micro-fracturing. These minerals include small hornblende grains, which themselves are enclosed within diopside aligned within the gneissic fabric. A second generation of gold is included in the same peak-metamorphic minerals but occurs along fine micro-fractures either as trails of fine equant or irregularly shaped grains or as fracture fill. In other words, the calc-silicate sample TH46 clearly illustrates that gold was present during early high-temperature events and partly remobilised during later D₃ low-temperature micro-fracturing (Le *et al.*, 2021a).

Temperature estimates for D₃ chlorite alteration

The chlorite thermometry results track the evolving temperature conditions during the alteration stages 2–4 during D₃. The results (Figure 10; Supplemental data, Table S1) indicate that the earlier chlorite types (*i.e.* chlorite₁ and chlorite₂; Figure 6a–c) display the widest compositional range (Table S1), suggesting continuous re-equilibration as retrograde conditions and fluid infiltration progressed during D₃. During the early D₃, stage 1 hornblende formed as randomly oriented grains in some of the quartz–feldspar mylonite units (Le *et al.*, 2021a). The appearance of hornblende in the stage 1 mineral assemblage from the D₃ metamorphism suggests that temperature conditions during stage 1 exceeded 500 °C. During stages 2–3, the main episodes of D₃ gold accumulation (Figure 6a, c; Le *et al.*, 2021a), the temperature estimate obtained from the compositionally variable grains of chlorite_{1–2} varied between 160 and 380 °C. This temperature range coincides with the widespread infiltration of oxidising hydrothermal fluids that reset most of oxygen isotope values of quartz in the area, producing a narrow range (+10.5 to +13.7‰ VSMOW) for most in quartz from different rock types (Le *et al.*, 2022). Chlorite₃ has a more homogeneous composition than chlorite_{1–2}, resulting in a narrow temperature range of 130–170 °C, which prevailed during stage 4 of D₃. This suggests that stage 4 represents a distinct hydrothermal alteration event, characterised by a separate suite of alteration minerals including calcite (Figure 6d) and some of the Pb–Cu–Bi selenides (Le *et al.*, 2021a).

During the 1525–1520 Ma D₃ metamorphic and hydrothermal event at Tick Hill area, gold formation/remobilisation can be tracked with chlorite thermometry in combination with *P–T* constraints imposed by mineral assemblages and the presence of Bi-selenides, as well as conditions obtained from oxygen isotope values in quartz (Le *et al.*, 2022). Temperatures would have peaked during stage 1 when hornblende–oligoclase–albite formed at temperatures slightly higher than ~500 °C. This temperature is comparable with the amphibolite facies metamorphism in southern Mary Kathleen and the Eastern Fold Belt (*e.g.* Abu Sharib & Sanislav, 2013; Withnall & Hutton, 2013). During later D₃ alteration, temperatures gradually decreased from ~380 to ~160 °C during stage 2 and stage 3, with a later low-temperature pulse during

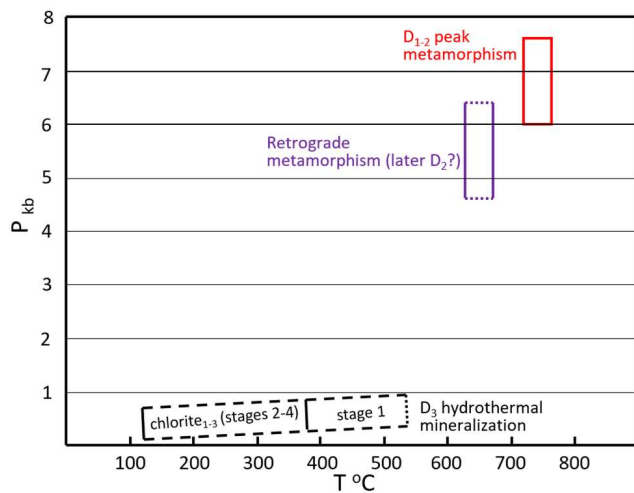


Figure 11. P - T diagram for D_{1-3} metamorphism-hydrothermal events in the Tick Hill Area. The pressure for retrograde metamorphism is unknown, while the pressure for D_3 hydrothermal events is assumed based on the occurrences of bismuth selenide. The temperature estimates for D_3 events are based on the presence of hornblende during stage 1 and temperature estimates for chlorite $_{1-3}$ formed during stages 2–4.

stage 4 when selenides precipitated with sulfides and calcite veins at temperatures as low as $\sim 130^\circ\text{C}$.

Conclusions

The compositions of a variety of mineral phases from Tick Hill constrain the P - T conditions during D_{1-3} . Critical assemblages that were analysed for P - T work include: (1) garnet–plagioclase–hornblende–biotite–quartz in the amphibolite gneiss, which preserves D_{1-2} peak-metamorphic conditions of 720 – 750°C and 6.0 – 7.6 kbar; (2) diopside–plagioclase–scapolite–hornblende in amphibole-rich calc-silicate, which preserves metamorphism conditions of 620 – 670°C , possibly owing to D_1 retrograde metamorphism or affected by the early stages of the D_3 overprint; and (3) D_3 chlorite that was associated with hydrothermal gold mineralisation and alteration formed from 380°C (stage 2) to 130°C (stage 4). Gold enrichment is associated with chlorite $_1$ and chlorite $_2$ (~ 380 to $\sim 160^\circ\text{C}$). Metamorphic temperatures during D_3 stage 1 may have reached temperatures of $>500^\circ\text{C}$ based on the coexistence of amphibole and oligoclase.

The migmatization textures and P - T estimates for the garnet-bearing amphibolite gneiss in the Tick Hill area indicate that high-grade metamorphism at 1790 – 1770 Ma is only locally preserved. In the Mary Kathleen Domain, the amphibolite–granulite facies metamorphism at Tick Hill is higher than the amphibolite facies metamorphic conditions of the northern Mary Kathleen and Eastern Fold Belt. Overall, the rocks underwent peak metamorphism at high temperatures and moderate pressures at deep crustal conditions during the early stages of D_1 deformation and low temperatures towards the end of D_3 (Figure 11).

Acknowledgements

We would like to thank the Geological Survey of Queensland (GSQ), the Economic Geology Research Centre (EGRU, JCU) and Rick Valenta,

who provided support to conduct this study. We would like to thank Peter Rea and Alex Brown from Glencore, Mount Isa Mines, and Paul Tan, Brett Davis and Rob Watkins from Carnaby Resources for providing logistical support during fieldwork, providing access to the drill core and mine site, and providing data sets. We would like to thank Nick Oliver for donating the Tick Hill samples for this study. We would like to thank the Ho Chi Minh University of Science for supporting the study project (code T2023-53) in comparing the SEM-based mineral thermometry with the EPMA-based one.

Disclosure statement

No potential conflict of interest was reported by the author(s).

Funding

Funding for this study was provided by the Department of Natural Resources, GSQ and the VNU-HCM University of Science, Ho Chi Minh, Vietnam under the study project code T2023-53.

ORCID

T. X. Le  <http://orcid.org/0000-0001-8137-1134>
 P. H. G. M. Dirks  <http://orcid.org/0000-0002-1582-1405>
 I. V. Sanislav  <http://orcid.org/0000-0002-3680-3740>
 J. M. Huizenga  <http://orcid.org/0000-0003-3254-702X>
 H. A. Cocker  <http://orcid.org/0000-0002-5543-5701>

Data availability statement

The geological map of the Tick Hill Area is mainly updated from the exploration maps (Rutherford, N. F., 2000), which can be found at <https://geoscience.data.qld.gov.au/report/cr031587>.

References

- Abu Sharib, A. S. A. A., & Sanislav, I. V. (2013). Polymetamorphism accompanied switching in horizontal shortening during Isan Orogeny: Example from the Eastern Fold Belt, Mount Isa Inlier, Australia. *Tectonophysics*, 587, 146–167. <https://doi.org/10.1016/j.tecto.2012.06.051>
- Anderson, J. L. (1996). Status of thermobarometry in granitic batholiths. *Earth and Environmental Science Transactions of the Royal Society of Edinburgh*, 87(1-2), 125–138. <https://doi.org/10.1017/S0263593300006544>
- Berman, R. (1990). Mixing properties of Ca–Mg–Fe–Mn garnets. *American Mineralogist*, 75(3-4), 328–344.
- Betts, P., Armit, R., Stewart, J., Aitken, A., Ailleres, L., Donchak, P., Hutton, L., Withnall, I., & Giles, D. (2016). Australia and Nuna. In Z. X. Li, D. A. D. Evans & J. B. Murphy (Eds.), *Supercontinent Cycles Through Earth History* (Vol. 424, pp. 47–81). Geological Society of London, Special Publication. <https://doi.org/10.1144/SP424.2>
- Blake, D., & Steward, A. (1992). Stratigraphic and tectonic framework, Mount Isa. *AGSO Bulletin*, 243, 1–11.
- Blundy, J. D., & Holland, T. J. (1990). Calcic amphibole equilibria and a new amphibole–plagioclase geothermometer. *Contributions to Mineralogy and Petrology*, 104(2), 208–224. <https://doi.org/10.1007/BF00306444>
- Bourdelle, F., & Cathelineau, M. (2015). Low temperature chlorite geothermometry: A graphical representation based on a $T-R_2 \pm Si$ diagram. *European Journal of Mineralogy*, 27(5), 617–626. <https://doi.org/10.1127/ejm/2015/0027-2467>
- Cathelineau, M. (1988). Cation site occupancy in chlorites and illites as a function of temperature. *Clay Minerals*, 23(4), 471–485. <https://doi.org/10.1180/claymin.1988.023.4.13>

- Cathelineau, M., & Nieva, D. (1985). A chlorite solid solution geothermometer. The Los Azufres (Mexico) geothermal system. *Contributions to Mineralogy and Petrology*, 91(3), 235–244. <https://doi.org/10.1007/BF00413350>
- Choy, D. K. W. (1994). *The geology, structure, petrology, alteration and mineralization of Tick Hill* [Unpublished master thesis]. Monash University. 220 p.
- Droop, G. T. R. (1987). A general equation for estimating Fe³⁺ concentrations in ferromagnesian silicates and oxides from microprobe analyses, using stoichiometric criteria. *Mineralogical Magazine*, 51(361), 431–435. <https://doi.org/10.1180/minmag.1987.051.361.10>
- Ellis, D. J., & Green, D. H. (1979). An experimental study of the effect of Ca upon garnet clinopyroxene Fe–Mg exchange equilibria. *Contributions to Mineralogy and Petrology*, 71(1), 13–22. <https://doi.org/10.1007/BF00371878>
- Essene, E. (1989). The current status of thermobarometry in metamorphic rocks. In J. S. Daly, R. A. Cliff & B. W. D. Yardley (Eds.), *Evolution of metamorphic belts* (Vol. 43, pp. 1–44). Geological Society Special Publication. <https://doi.org/10.1144/GSL.SP.1989.043.01.02>
- Essene, E. J. (2009). Thermobarometry gone astray. In A. K. Gupta & S. Dasgupta (Eds.), *Physics and chemistry of the earth's interior, crust, mantle and core* (pp. 101–133). Indian National Academy.
- Essene, E. J., & Peacor, D. R. (1995). Clay mineral thermometry: A critical perspective. *Clay Minerals*, 43, 728–745. <https://doi.org/10.1346/CCMN.1995.0430504>
- Esteban, J. J., Cuevas, J., Tubía, J. M., Liati, A., Seward, D., & Gebauer, D. (2007). Timing and origin of zircon-bearing chlorite schists in the Ronda peridotites (Betic Cordilleras, S Spain). *Lithos*, 99(1–2), 121–135. <https://doi.org/10.1016/j.lithos.2007.06.006>
- Ferry, J. T., & Spear, F. (1978). Experimental calibration of the partitioning of Fe and Mg between biotite and garnet. *Contributions to Mineralogy and Petrology*, 66(2), 113–117. <https://doi.org/10.1007/BF00372150>
- Ganguly, J., & Kennedy, G. C. (1974). The energetics of natural garnet solid solution. *Contributions to Mineralogy and Petrology*, 48(2), 137–148. <https://doi.org/10.1007/BF00418615>
- Gillis, K. M., Muehlenbachs, K., Stewart, M., Karson, J., & Gleeson, T. (2001). Fluid flow patterns in fast-spreading East Pacific Rise crust exposed at Hess Deep. *Journal of Geophysical Research: Solid Earth*, 106(B11), 26311–26329. <https://doi.org/10.1029/2000JB000038>
- Graham, C. M., & Powell, R. (1984). A garnet–hornblende geothermometer: Calibration, testing, and application to the Pelona Schist, Southern California. *Journal of Metamorphic Geology*, 2(1), 13–31. <https://doi.org/10.1111/j.1525-1314.1984.tb00282.x>
- Hodges, K., & Spear, F. S. (1982). Geothermometry, geobarometry and the Al₂SiO₅ triple point at Mount Moosilauke, New Hampshire. *American Mineralogist*, 67(11–12), 1118–1134.
- Holland, T., & Blundy, J. (1994). Non-ideal interactions in calcic amphiboles and their bearing on amphibole–plagioclase thermometry. *Contributions to Mineralogy and Petrology*, 116(4), 433–447. <https://doi.org/10.1007/BF00310910>
- Inoue, A., Meunier, A., Patrier-Mas, P., Rigault, C., Beaufort, D., & Vieillard, P. (2009). Application of chemical geothermometry to low-temperature trioctahedral chlorites. *Clays and Clay Minerals*, 57(3), 371–382. <https://doi.org/10.1346/CCMN.2009.0570309>
- Jercinovic, M. J., Williams, M. L., & Lane, E. D. (2008). In-situ trace element analysis of monazite and other fine-grained accessory minerals by EPMA. *Chemical Geology*, 254(3–4), 197–215. <https://doi.org/10.1016/j.chemgeo.2008.05.016>
- Jowett, E. C. (1991). *Fitting iron and magnesium into the hydrothermal chlorite geothermometer* [Paper presentation]. GAC/MAC/SEG Joint Annual Meeting (Tront), Abstract, A62. <https://doi.org/10.2139/ssrn.3863523>
- Kohn, M. J., & Spear, F. S. (1989). Empirical calibration of geobarometers for the assemblage garnet + plagioclase + quartz. *American Mineralogist*, 74(1–2), 77–84.
- Kohn, M. J., & Spear, F. S. (1990). Two new geobarometers for garnet amphibolites, with applications to southeastern Vermont. *American Mineralogist*, 75(1–2), 89–96.
- Laverne, C., Vanko, D. A., Tararotti, P., & Alt, J. C. (1995). Chemistry and geothermometry of secondary minerals from the deep sheeted dike complex, Hole 504B1. *Paper Presented at the Proceedings of the Ocean Drilling Program, Scientific Results*.
- Le, T. X., Dirks, P. H. G. M., Sanislav, I. V., Harris, C., Huizenga, J. M., Cocker, H., & Manestar, G. N. (2022). Quartz oxygen isotopes from Tick Hill Area in Mount Isa Inlier – Indication of a regional fluid overprint. *Australian Journal of Earth Sciences*, 69(3), 439–452. <https://doi.org/10.1080/08120099.2022.1985608>
- Le, T. X., Dirks, P. H. G. M., Sanislav, I. V., Huizenga, J. M., Cocker, H., & Manestar, G. N. (2021a). Geological setting and mineralisation characteristics of the Tick Hill Gold Deposit, Mount Isa Inlier, Queensland, Australia. *Ore Geology Reviews*, 137, 104288. <https://doi.org/10.1016/j.oregeorev.2021.104288>
- Le, T. X., Dirks, P. H. G. M., Sanislav, I. V., Huizenga, J. M., Cocker, H., & Manestar, G. N. (2021b). Geochronological constraints on the geological history and gold mineralisation in the Tick Hill region, Mount Isa Inlier. *Precambrian Research*, 366, 106422. <https://doi.org/10.1016/j.precamres.2021.106422>
- Moura, M. A., Botelho, N. F., Olivo, G. R., & Kyser, T. K. (2006). Granite-related Paleoproterozoic, Serrinha gold deposit, southern Amazonia, Brazil: Hydrothermal alteration, fluid inclusion and stable isotope constraints on genesis and evolution. *Economic Geology*, 101(3), 585–605. <https://doi.org/10.2113/gsecongeo.101.3.585>
- Newton, R. C., Charlu, T. V., & Kleppa, O. J. (1977). Thermochemistry of high pressure garnets and clinopyroxenes in the system CaO–MgO–Al₂O₃–SiO₂. *Geochimica et Cosmochimica Acta*, 41(3), 369–377. [https://doi.org/10.1016/0016-7037\(77\)90264-2](https://doi.org/10.1016/0016-7037(77)90264-2)
- Oliver, N. (1995). Hydrothermal history of the Mary Kathleen Fold Belt, Mount Isa Block, Queensland. *Australian Journal of Earth Sciences*, 42(3), 267–279. <https://doi.org/10.1080/08120099508728201>
- Perchuk, L. (1967). Analysis of thermodynamic conditions of mineral equilibria in amphibole–garnet rocks. *Izvestiya Akademii Nauk SSSR, Seriya Geologicheskaya*, 3, 57–83.
- Perchuk, L. (1969). The effect of temperature and pressure on the equilibrium of natural iron–magnesium minerals. *International Geology Review*, 11(8), 875–901. <https://doi.org/10.1080/00206816909475127>
- Perchuk, L. L. (1970). *Equilibria of Rock-Forming Minerals*. 'Nauka' Press. (in Russian)
- Perchuk, L., & Lavrent'eva, I. (1983). Experimental investigation of exchange equilibria in the system cordierite–garnet–biotite. In S. K. Saxena (Ed.), *Kinetics and equilibrium in mineral reactions. Advances in physical geochemistry* (Vol. 3, pp. 199–239). Springer. https://doi.org/10.1007/978-1-4612-5587-1_7
- Perchuk, L. L., Aranovich, L. Y., Podlesskii, K. K., Lavrant'eva, I. V., Gerasimov, V. Y., Fed'kin, V. V., Kitsul, V. I., Karsakov, L. P., & Berdnikov, N. V. (1985). Precambrian granulites of the Aldan shield, eastern Siberia, USSR. *Journal of Metamorphic Geology*, 3(3), 265–310. <https://doi.org/10.1111/j.1525-1314.1985.tb00321.x>
- Poli, S., & Schmidt, M. W. (1992). A comment on “Calcic amphibole equilibria and a new amphibole–plagioclase geothermometer” by J. D. Blundy & T. J. B. Holland. *Contributions to Mineralogy and Petrology*, 111(2), 273–278. <https://doi.org/10.1007/BF00348960>
- Powell, R. (1985). Regression diagnostics and robust regression in geothermometer/geobarometer calibration: The garnet clinopyroxene geothermometer revisited. *Journal of Metamorphic Geology*, 3(3), 231–243. <https://doi.org/10.1111/j.1525-1314.1985.tb00319.x>
- Ravna, E. K. (2000). Distribution of Fe²⁺ and Mg between coexisting garnet and hornblende in synthetic and natural systems: An empirical calibration of the garnet–hornblende Fe–Mg geothermometer. *Lithos*, 53(3–4), 265–277. [https://doi.org/10.1016/S0024-4937\(00\)00029-3](https://doi.org/10.1016/S0024-4937(00)00029-3)
- Ridolfi, F., Zanetti, A., Renzulli, A., Perugini, D., Holtz, F., & Oberti, R. (2018). AMFORM, a new mass-based model for the calculation of the unit for-

- mula of amphiboles from electron microprobe analyses. *American Mineralogist*, 103(7), 1112–1125. <https://doi.org/10.2138/am-2018-6385>
- Rutherford, N. F. (2000). *Second annual joint venture report to 1st January 2000 for exploration permits for minerals 9083, 11012 & 11013, Burke River Region, Mount Isa-Cloncurry District, North West Queensland, Technical Report No: 2. Queensland Geological Survey*. <https://geoscience.data.qld.gov.au/report/cr031587>
- Spear, F. S. (1980). NaSi \rightleftharpoons CaAl exchange equilibrium between plagioclase and amphibole. *Contributions to Mineralogy and Petrology*, 72(1), 33–41. <https://doi.org/10.1007/BF00375566>
- Spear, F. S. (1981). Amphibole–plagioclase equilibria: An empirical model for the relation albite+tremolite=edenite + 4 quartz. *Contributions to Mineralogy and Petrology*, 77(4), 355–364. <https://doi.org/10.1007/BF00371564>
- Spear, F. S. (1993). *Metamorphic phase equilibria and pressure–temperature–time paths* (p. 99). Mineralogical Society of America.
- Spear, F. S., & Kohn, M. J. (1999). *Program thermobarometry. GTB software*. Provided by the Spear 2021.
- Spence, J. S., Sanislav, I. V., & Dirks, P. H. (2021). 1750–1710 Ma deformation along the eastern margin of the North Australia Craton. *Precambrian Research*, 353, 106019. <https://doi.org/10.1016/j.precamres.2020.106019>
- Spence, J. S., Sanislav, I. V., & Dirks, P. H. (2022). Evidence for a 1750–1710 Ma orogenic event, the Wonga Orogeny, in the Mount Isa Inlier, Australia: Implications for the tectonic evolution of the North Australian Craton and Nuna Supercontinent. *Precambrian Research*, 369, 106510. <https://doi.org/10.1016/j.precamres.2021.106510>
- Tedman-Jones, C. (2001). *Tick Hill core relogging review* (Internal report to MIM Exploration Pty Ltd. Misc.2001/010, Record No. 30764). Mount Isa Exploration Office.
- Thomas, H., & Rana, H. (2020). Garnet–hornblende geothermometer: A comparative study. *Journal of the Geological Society of India*, 96(6), 591–596. <https://doi.org/10.1007/s12594-020-1607-9>
- Thompson, A. B. (1976). Mineral reactions in pelitic rocks; II, Calculation of some PTX (Fe–Mg) phase relations. *American Journal of Science*, 276(4), 425–454. <https://doi.org/10.2475/ajs.276.4.425>
- Timpa, S., Gillis, K. M., & Canil, D. (2005). Accretion-related metamorphism of the Metchosin igneous complex, southern Vancouver Island British Columbia. *Canadian Journal of Earth Sciences*, 42(8), 1467–1479. <https://doi.org/10.1139/e05-043>
- Vidal, O., de Andrade, V., Lewin, E., Munoz, M., Parra, T., & Pascarelli, S. (2006). P–T-deformation-Fe³⁺/Fe²⁺ mapping at the thin section scale and comparison with XANES mapping: Application to a garnet-bearing metapelite from the Sambagawa metamorphic belt (Japan). *Journal of Metamorphic Geology*, 24(7), 669–683. <https://doi.org/10.1111/j.1525-1314.2006.00661.x>
- Vidal, O., Lanari, P., Munoz, M., Bourdelle, F., & De Andrade, V. (2016). Deciphering temperature, pressure, and oxygen activity conditions of chlorite formation. *Clay Minerals*, 51(4), 615–633. <https://doi.org/10.1180/claymin.2016.051.4.06>
- Withnall, I., & Hutton, L. (2013). Chapter 2: North Australian Craton. In P. A. Jell (Ed.), *Geology of Queensland* (pp 23–112). Geological Survey of Queensland.
- Wyborn, L. A. I. (1997). Dajarra 1:100,000 digital geology, *part of Mount Isa geological digital dataset*. Updated by Geological Survey of Queensland 2011, 2015 and 2018. <http://pid.geoscience.gov.au/dataset/ga/30923>
- Yavuz, F., Kumral, M., Karakaya, N., Karakaya, M. Ç., & Yıldırım, D. K. (2015). A Windows program for chlorite calculation and classification. *Computers & Geosciences*, 81, 101–113. <https://doi.org/10.1016/j.cageo.2015.04.011>
- Zang, W., & Fyfe, W. S. (1995). Chloritisation of the hydrothermally altered bedrock at the Igarapé Bahia gold deposit, Carajás, Brazil. *Mineralium Deposita*, 30(1), 30–38. <https://doi.org/10.1007/BF00208874>